Bioconjugate Chemistry

ACS AUTHORCHOICE

pubs.acs.org/bc Article

Probing Biomolecular Interactions by a Pattern-Forming Peptide–Conjugate Sensor

Tamara Heermann, Henri G. Franquelim, Philipp Glock, Leon Harrington, and Petra Schwille*

Cite This: *Bioconjugate Chem.* 2021, 32, 172–181 Read Online

ACCESS | Metrics & More | Article Recommendations | Supporting Information

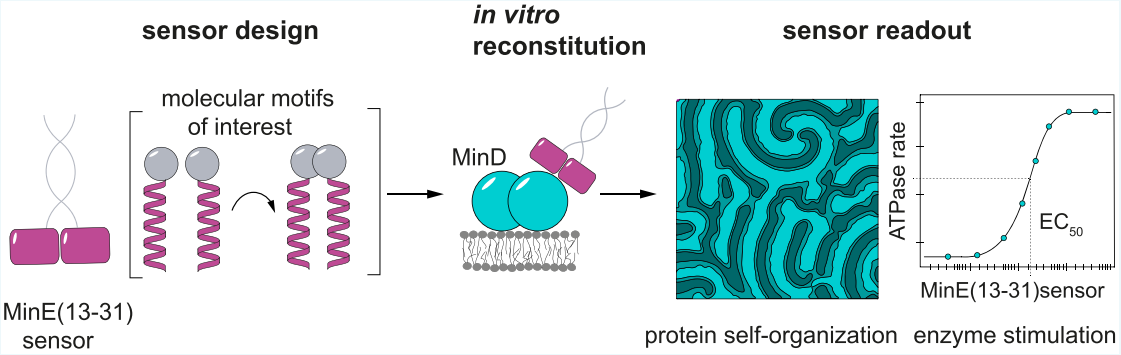

ABSTRACT: As a key mechanism underpinning many biological processes, protein self-organization has been extensively studied. However, the potential to apply the distinctive, nonlinear biochemical properties of such self-organizing systems to biotechnological problems such as the facile detection and characterization of biomolecular interactions has not yet been explored. Here, we describe an *in vitro* assay in a 96-well plate format that harnesses the emergent behavior of the *Escherichia coli* Min system to provide a readout of biomolecular interactions. Crucial for the development of our approach is a minimal MinE-derived peptide that stimulates MinD ATPase activity only when dimerized. We found that this behavior could be induced via any pair of foreign, mutually binding molecular entities fused to the minimal MinE peptide. The resulting MinD ATPase activity and the spatiotemporal nature of the produced protein patterns quantitatively correlate with the affinity of the fused binding partners, thereby enabling a highly sensitive assay for biomolecular interactions. Our assay thus provides a unique means of quantitatively visualizing biomolecular interactions and may prove useful for the assessment of domain interactions within protein libraries and for the facile investigation of potential inhibitors of protein–protein interactions.

Numerous different biological and biophysical techniques are available to detect and characterize molecular interactions both *in vivo*, for example, split fluorescent reporters[1] and yeast two-hybrid/mating systems;[2,3] as well as *in vitro,* such as fluorescence correlation spectroscopy (FCS), Förster resonance energy transfer (FRET), AlphaScreen,[4] light scattering, and isothermal titration calorimetry (ITC), among others.[5] Despite the range of methods available, it remains challenging to obtain *in vitro* a facile direct readout of the presence and strength of interactions while screening in a high-throughput manner, in particular, when using concentrations in the nanomolar range. One phenomenon that has not, to our knowledge, been harnessed for biomolecular interaction screening but which has the potential to provide a visual readout is protein pattern formation. Indeed, it has recently been discovered that protein pattern formation can be engineered by combining specific, interacting protein domains in the self-organizing *Escherichia coli* Min protein system, which suggests the potential of this system to be employed as a unique sensor for biomolecular interactions.[6]

Molecular self-organization into emergent patterns is ubiquitous in nature, and underpins essential functions across all scales of life.[7] One of the best-studied systems known to exhibit pattern formation is the Min system,[8] consisting of three proteins: MinC, MinD, and MinE. It is essential for the spatiotemporal regulation of the positioning of the division ring component FtsZ to midcell and is remarkably simple, given that only two protein components are required for pattern formation. Further, the key functional components have been found to be amenable to engineering. In particular, the ATPase-activating protein MinE has been the target of several mutation studies to understand the structure–function relationship of its domains and has recently been successfully

Received: November 3, 2020
Revised: November 30, 2020
Published: December 14, 2020

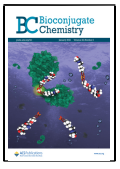

https://dx.doi.org/10.1021/acs.bioconjchem.0c00596
Bioconjugate Chem. 2021, 32, 172–181

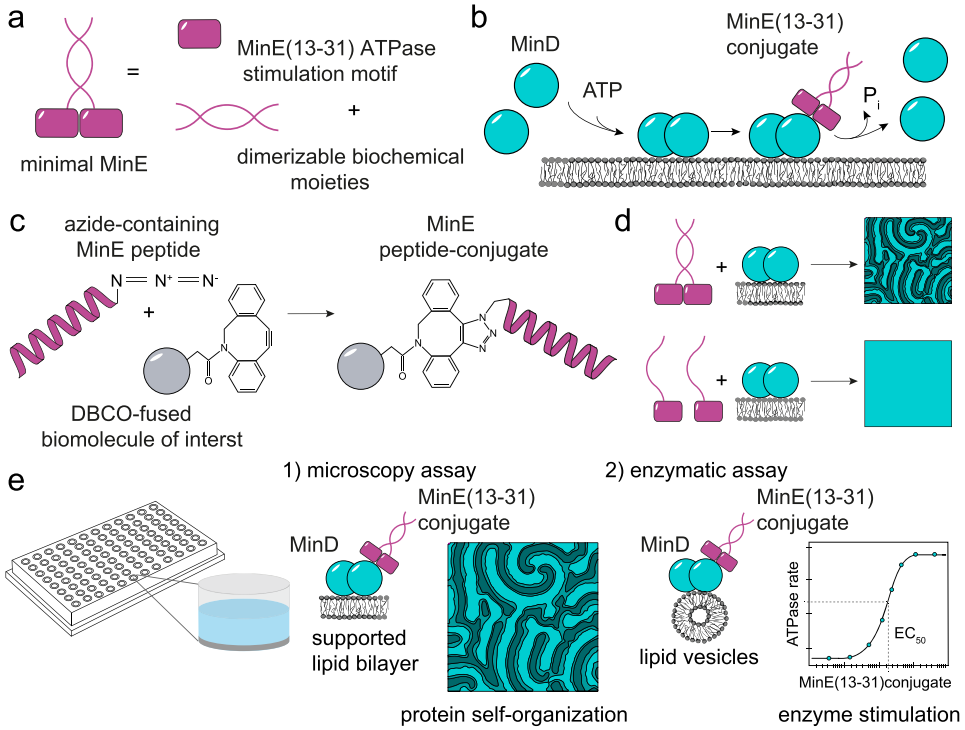

Figure 1. A minimal MinE peptide couples dimerization of biomolecules of interest into self-organized protein patterns. (a) Schematic illustration of a minimal MinE comprising the MinE(13−31) helical peptide that interacts with MinD to stimulate its ATPase activity and a biochemical moiety that is able to dimerize with a counterpart or with itself. (b) Simplified representation of the MinDE self-organization mechanism on a planar bilayer. Upon ATP-binding, cytosolic MinD (cyan) dimerizes, localizes to the membrane, and locally enhances protein self-recruitment (positive feedback). After binding a dimerized MinE(13−31) peptide conjugate (magenta), ATP hydrolysis is stimulated, which leads to the dissociation of MinD from the membrane. (c) Schematic illustrating the conjugation strategy, wherein the azide-containing MinE peptide and the DBCO-fused biomolecule are coupled via copper-free click-chemistry to form the MinE peptide conjugate used in the assays described herein. (d) Fusion constructs of the minimal MinE peptide with domains able to form a homo- or heterodimer stimulate MinD ATPase activity upon dimerization and thus induce MinD self-organization into protein patterns (upper panel). If the MinE peptide is instead attached to domains that do not interact, MinD ATPase activity is not stimulated, and a homogeneous protein carpet is observed (lower panel). (e) Schematic representation of two assays performed in this study to test for a potential interaction of two biochemical domains, where each domain is fused to the MinE(13−31) peptide. Microscopy assay—assessment of MinD self-organization in response to the addition of the examined peptide-fusion constructs. Enzymatic assay—determination of the half maximal stimulation of MinD ATPase activity with regard to fusion construct concentration.

reduced to a minimal, pattern-inducing entity.[6,9,10] MinE comprises four functional motifs: a membrane targeting sequence (MTS), a conformational switch enabling the exchange of an open (active) and a closed (inactive) arrangement, a dimerization interface, and a short α-helical peptide that activates MinD ATPase activity.[6,10,11] Intriguingly, the ATPase-activating peptide in combination with either the MTS or any moiety capable of dimerization is sufficient to induce MinD pattern formation.[6] It is thus tempting to extrapolate the functionality of dimerization even beyond the protein context.

Specifically, in this work we demonstrate the application of a MinE derived peptide (*E. coli* aa 13−31), or minimal MinE, as a generic sensor to couple dimerization of biomolecules to the dynamics of the MinDE pattern forming system.[6] By fusing putative interaction partners to the minimal MinE peptide, we take advantage of the fact that only a peptide dimer is able to stimulate MinD ATPase activity and thereby induce MinD pattern formation. As proof-of-concept for our synthetic peptide-based approach, we use complementary single-stranded DNA "handles" that can be easily modulated to a wide range of affinities. We show that hybridized dsDNA−peptide conjugates faithfully induce pattern formation. Further, competing DNA strands that are not conjugated to the minimal MinE peptide can be used to deplete active minimal MinE dimers and thereby terminate pattern formation, rendering the readout reversible.

The sensor can be operated quantitatively, as the affinity of the peptide-conjugated interaction partners determines both the spatiotemporal nature of the emergent pattern, and the concentration required for half-maximal MinD ATPase stimulation. We further demonstrate the utility of our assay by testing two additional systems of interaction partners: basic Leucine Zipper Domains (bZIP) and biotin−streptavidin. Our novel protein self-organization-based assay is thus broadly applicable and scalable, and provides a unique readout of biochemical interactions.

RESULTS AND DISCUSSION

An α-Helical MinE Peptide Dimer Is a Generic Sensor for Molecular Interactions. The first functional element of our assay system is a short α-helical sequence (aa 13−31) derived from *E. coli* MinE, which is essential for the stimulation of MinD ATPase activity.[6,10] As MinD is only stimulated by dimers of MinE bearing two copies of said α-helical peptide, the second functional element is a pair of interacting moieties (Figure 1a). Potentially any type of peptide-conjugated

https://dx.doi.org/10.1021/acs.bioconjchem.0c00596
Bioconjugate Chem. 2021, 32, 172−181

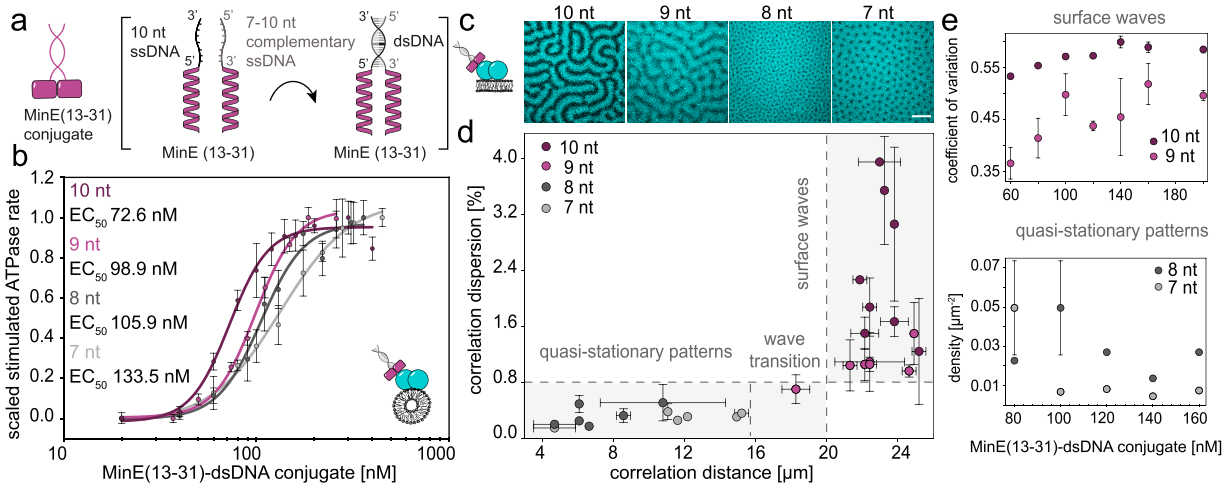

Figure 2. Complementary ssDNA handles used as tunable-affinity interaction pairs demonstrate distinct differences in protein self-organization for MinE(13−31)-dsDNA conjugates with different affinities. (a) Schematic illustration of a minimal MinE conjugate with ssDNA handles as the dimerization moiety. This conjugate design allows variants with different binding affinities to be readily generated via hybridization of a common peptide-coupled 10 nt handle with complementary strands of varying lengths (7−10 nt). (b) Response of MinD ATPase activity (1 μM) to increasing concentrations of the common 10 nt peptide in combination with complementary 10 nt (dark purple; EC_{50} − 72.6 nM with a 95% CI of 68.0 to 77.5 nM), 9 nt (purple; EC_{50} − 98.9 nM with a 95% CI of 95.2 to 102.7 nM), 8 nt (light purple; EC_{50} − 105.9 nM with a 95% CI of 98.9 to 113.4 nM), or 7 nt (light mauve; EC_{50} − 133.5 nM with a 95% CI of 119.0 to 149.8 nM) peptide conjugates. Plotted values represent the mean ± SD of two independent experiments, each comprising three technical replicates. (c) Representative fluorescence microscopy images of 1 μM MinD (30% ATTO655-KCK-MinD) reconstituted with 140 nM of the common 10 nt peptide conjugate in combination with the 10, 9, 8, or 7 nt complementary strands fused to the MinE(13−31) peptide. Scale bars represent 40 μm. (d) Classification of the obtained *in vitro* reconstituted protein patterns according to the correlation distance and the determined correlation dispersion. Each two replicates per MinE(13−31)−dsDNA conjugate pair and concentration were analyzed (data representation: mean ± SD) and a visual overview of the obtained patterns is shown in Figure S4a. For simplicity, images displaying no patterns were excluded for every conjugate pair (correlation distance below 4 μm). (e) Discrimination of surface waves and quasi-stationary patterns by either plotting the coefficient of variation (upper panel) or the correlation density (lower panel) against the respective MinE(13−31)−dsDNA conjugate concentration. Data represents the mean ± SD value of two independent replicates.

biomolecule can be used to drive dimerization of the minimal MinE peptide (Figure 1c). Thus, when reconstituted on a supported lipid bilayer, the customizable minimal MinE, just like its native counterpart, will stimulate the ATPase activity of membrane-attached, ATP-bound MinD (Figure 1b). Nucleotide hydrolysis leads, in turn, to the detachment of MinD from the lipid membrane, and the continuous cycling of this mechanism gives rise to protein self-organization and pattern formation.[12,13] At first, this system might appear complex; however, one can appreciate the distinct output, as pattern formation is only possible if the moieties of interest, fused to the minimal MinE peptide, are able to interact (Figure 1d). In contrast, non-interacting moieties result in homogeneous MinD membrane coverage, deficient in ATP hydrolysis. As well as the optical readout provided by pattern formation, the stimulation of MinD ATPase activity can be measured as an alternative spectroscopic readout. Like the microscopy assay, this approach can be scaled into a multiwell plate format to allow high-throughput screening (Figure 1e).

Stimulated MinD Patterns Are Dependent on the Affinity of the Binding Partners. As a proof-of-concept, and to explore the range of binding affinities that can be determined with our assay, we began by using DNA hybridization as a well-characterized system that allows the design of interacting partners with varying affinity constants. In our design, complementary single-stranded DNA (ssDNA) handles, each with a two-nucleotide spacer preceding the hybridizing bases, are fused to the α-helical MinE peptide via copper-free click chemistry. We used a 10-nucleotide-long handle as a common binding partner, while progressively reducing the length of the complementary strand by one nucleotide each (Figure 2a; Figure S1, Table S3). This allowed us to assess the effect of varying the thermodynamic potential energies (Gibbs free energy, ΔG; Table S2) of DNA hybridization within our MinE constructs on emerging MinD self-organization.

As shown in Figure 2c, we found that hybridization of the common 10 nt-peptide (c10 nt) with its complementary 10 nt counterpart (upper row) induced protein pattern formation in the form of traveling surface waves (Figures S4a and S2). As for previous studies, concentrations in the low nanomolar range of the minimal MinE were sufficient for MinD stimulation.[6,11] Considering the structural rearrangements required in WT MinE for MinD stimulation, namely, a shift from the latent/closed conformation to an active/open conformation, overactivity of the minimal MinE construct is not necessarily surprising, as conformational freedom of the contact helix already exists *ab initio*.[14,15] Hence, the helical dominance and consequently always active conformation exhibited by our minimal MinE construct in fact represents a particular advantage in our *in vitro* assay, because it allows us to examine low concentrations of reactants, in contrast to other techniques such as ITC.[16]

As with the patterns induced by the minimal MinE-dsDNA (c10 nt/10 nt) construct, chaotic spatial dynamics that evolved into propagating waves were observed for the corresponding version with a 9-nucleotide overlap (Figure 2c, Figure S4a). However, one can clearly recognize a delayed onset of pattern formation and diffuse, rather than defined, MinD concentration gradients. Intriguingly, further reduction of the DNA-

https://dx.doi.org/10.1021/acs.bioconjchem.0c00596
Bioconjugate Chem. 2021, 32, 172−181

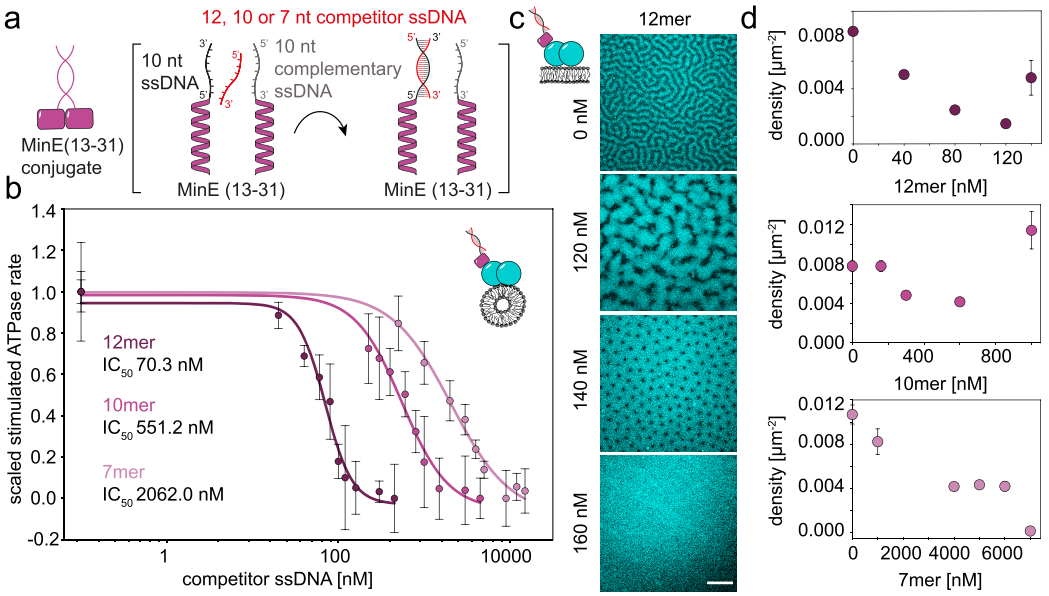

Figure 3. Receding protein self-organization can be used to assess the strength of an inhibitory agent on a dimerized moiety fused to the MinE(13−31) peptide. (a) Simplified schematic of the model assay design, which was used to test the ability of unmodified ssDNA to outcompete protein self-organization due to the binding and thus sequestration of the common 10 nt peptide, thereby preventing formation of the dsDNA complex with its complementary 10 nt conjugate partner. (b) Inhibition of MinD ATPase activity in response to the addition of the three tested competitor ssDNAs: 12-mer (dark purple; IC_{50} − 70.3 nM with a 95% CI of 60.3 to 81.9 nM), 10-mer (purple, IC_{50} − 551.2 nM with a 95% CI of 393.6 to 772.0 nM), 7-mer (mauve; IC_{50} − 2062.0 nM with a 95% CI of 1557.0 to 2730.0 nM). Plotted values represent the mean ± SD of two independent assays, each comprising three technical replicates. (c) Exemplary fluorescence microscopy images displaying the alteration, and ultimately abolition, of protein patterns formed by 1 μM MinD (30% ATTO655-KCK-MinD) and a dsDNA−peptide conjugate (common 10 nt and complementary 10 nt conjugates; 160 μM each) in response to increasing amounts of a ssDNA competitor with a complementary sequence to the common 10 nt peptide conjugate (12-mer, 12 overlaps). Scale bars represent 40 μm. (d) Discrimination of the dsDNA−peptide conjugate (common 10 nt and complementary 10 nt conjugates; 160 μM each) pattern density in response to the addition of varying concentrations of ssDNA competitor (12 overlaps; upper row), 10-mer (8 overlaps; middle row) or 7-mer (5 overlaps; bottom row). A visual overview of all analyzed patterns is shown in Figure S8. Data represents the mean ± SD value of two independent replicates.

strand overlap (8 and 7 nt) transformed the induced spatial arrangement into quasi-stationary patterns that resemble a hexagonal net or spots with a regular periodic distribution. The emergence of this type of Turing-like pattern is characterized by the uneven abundance of the two reactants, MinD and the minimal MinE-fusion construct, which correlates well with a decreased amount of dimerized DNA−peptide conjugates, due to the reduced affinity (or decreased ΔG) of the ssDNA handles.[17,18] In other words, low affinity between the conjugated domains might decrease the disintegration time of the formed MinE-dsDNA complex and thus effectively alters the amount of active minimal MinE.

In order to automate the optical readout of the induced protein patterns for high-throughput screening, we also designed an image analysis pipeline that allows the unbiased evaluation of protein self-organization according to the observed pattern types. As shown in Figure 2d, we were able to cluster the induced patterns into two main categories that enable the direct assessment of moiety binding strength: 1. stationary patterns, and 2. traveling waves. Based on the analysis of both spatial autocorrelation distance and dispersion, weak peptide-fused moieties only induce quasi-stationary patterns, being defined as having an autocorrelation distance of 4 to 16 μm and an autocorrelation dispersion of <0.8%. In contrast, strong interactions between the biomolecules of interest will lead to traveling surface waves and possess an autocorrelation distance >20 μm and an autocorrelation dispersion of >0.8%. Accordingly, both the 10 and 9 nt overlap minimal MinE-dsDNA constructs were assigned to the wave regime, whereas the 8 and 7 nt versions were assigned as quasi-stationary patterns. The great advantage of this image analysis pipeline is thus the ability to mostly assess the interaction strength of the fused moieties with a single experiment, thus reducing both material and time expenses. Although the above approach already enabled the main classification of intramolecular MinE-dsDNA affinities, we wanted to further quantify the MinD-antagonist strength within one cluster. For the wave regime (strong interaction), we thus analyzed the coefficient of variation (CoV), the normalized variance calculated over the entire image, and hence a measure of the relative contrast. Based on the sharp boundaries between local maxima and minima of pattern densities for the 10 nt MinE-dsDNA construct, we found the latter to possess higher CoV values compared to the weaker 9 nt version (Figure 2e, upper panel). In light of the reduced presence of anisotropic arrangement found in quasi-stationary patterns (weak interaction), we evaluated the pattern density, rather than the CoV, to distinguish between the higher arrangement frequency of the 8 nt compared to the 7 nt MinE-dsDNA construct (Figure 2e, lower panel).

To complement the use of pattern onset (Figure S4b) and phenotype as a semiquantitative optical readout of intermolecular affinity of the binding moieties of interest, we also investigated MinD ATPase stimulation as a direct quantitative readout. At a qualitative level, all examined peptide−DNA pairs stimulated ATP hydrolysis by MinD, dependent on their respective concentrations (Figure 2b). However, significant differences were observed when considering curve progression

https://dx.doi.org/10.1021/acs.bioconjchem.0c00596
Bioconjugate Chem. 2021, 32, 172−181

and halfway response (EC_{50}) of enzyme stimulation as quantitative parameters for the affinity between the binding moieties of interest. For example, the EC_{50} value determined for the peptide−DNA conjugate pair with 7 nt overlap was 134 nM (95% confidence interval (CI): 119.0 to 149.8 nM), whereas the EC_{50} for the 10 nt overlap pair was determined to be only 73 nM (95% CI: 68.01 to 77.51 nM). To further validate our observations, we calculated the Gibbs free energy for the different complementary DNA pairs, plotted these energies against the corresponding logarithmic EC_{50} values, and found them to be linearly correlated (Figure S3). We therefore conclude that EC_{50} values determined with our *in vitro* assay are a suitable approximation for interaction affinities.

To ensure that protein self-organization was indeed only induced after hybridization of the ssDNA handles, we also examined the effect of the unmodified α-helical MinE peptide and the single ssDNA−peptide conjugates on pattern-formation and ATPase stimulation (Figures S5, S6). Consistent with Glock et al., the unconjugated peptide did not promote MinD self-organization, due to the lack of MinE recruitment by membrane-bound MinD.[6,19] However, enzyme-stimulation-dependent ATP consumption was found to be slightly elevated, which might reflect the effect of limited peptide self-assembly/aggregation through cross-β-structure formation.[20] Similarly, single, unhybridized ssDNA-conjugates exhibited negligible ATPase stimulation and were unable to support pattern formation (Figure S6).

In summary, pattern analysis and EC_{50} values for MinD stimulation can be used as semiquantitative and quantitative parameters, respectively, to assess the strength of intramolecular affinities for the binding partners of interest in the studied peptide conjugates.

Competitor ssDNA Abolishes Minimal-MinE−Peptide Conjugate-Stimulated Self-Organization of MinD. Beyond screening for biomolecular interactions, it is important to be to able identify disruptors of pathological interaction pairs, such as those found in the dysregulation of cellular proliferation.[21] In general, putative drug targets are examined with *in vitro* inhibition assays that are differentiated into two categories: the ELISA-type and the mix-and-read assays. The latter category in fact represents the appropriate allocation for our novel protein self-organization based screen, as extensive experimental steps are avoided by the simple mixing of the required compounds, thus allowing the analysis of a wide dynamic range in a high-throughput manner.[22]

Conceptually, our inhibitor screen operates on the same principles as the interaction assay described earlier. However, instead of observing protein self-organization or measuring ATPase activity induced by the dimerization of peptide-fused moieties, one observes the concentration-dependent dispersal of protein patterns mediated by putative antagonists of the binding biomolecules of interest. To demonstrate this application, we again took advantage of the simplicity of short DNA duplexes as model interaction partners. Specifically, we used the same minimal MinE-DNA conjugate, comprising the common 10 nt peptide and the corresponding complementary partner to stimulate MinD activity. To detect binding inhibition, however, we added unconjugated ssDNA sequences that are complementary to the common 10-nt-peptide fusion construct (Figure 3a, Figure S7). Thus, the ssDNA competitors were expected to decrease the amount of functional minimal MinE-conjugate dimers and thereby inhibit stimulation of MinD.

We began by designing a particularly strong ssDNA competitor with an increased complementary sequence length compared to the respective 10 nt peptide fusion construct. Thus, very low concentrations of this antagonist, hereafter referred to as 12-mer, should have a marked effect on pattern formation due to the potent and fast depletion of active MinE-conjugates through strand displacement. Indeed, we observed a clear transformation from propagating surface waves, through quasi-stationary patterns (reverse hexagons), to the complete abolition of protein patterns in response to increasing amounts of the strongest tested ssDNA competitor (Figure 3c). A consistent effect on MinD ATPase activity was also observed, with a half-maximal inhibitory concentration (IC_{50}) of 70.3 nM, 95% CI of 60.3 to 81.9 nM, for the 12-mer (Figure 3b).

Having established that our assay could detect strong antagonists for the model DNA duplex, we also tested the sensitivity of the assay for weaker modulators. We found that the addition of a 10 nt (10-mer, Figure S8, middle panel) or 7 nt (7-mer, lower panel) ssDNA inhibitor led to the abolition of MinD self-organization, but only at higher concentrations in comparison to the 12-mer. Rather than altering the type of pattern observed, as seen with the 12-mer, higher 10-mer and 7-mer modulator concentrations instead lead to altered wavelengths of the protein patterns, before eventually abolishing them completely. With regard to this observation, we suspect that similar or weaker affinities between the inhibitor and the complementary ssDNA−peptide conjugate lead to strand replacement reactions with the peptide conjugates on a similar or reduced time scale as dimerization of the complementary peptide−ssDNA pairs. Thus, only significantly higher inhibitor concentrations, relative to the functional minimal MinE−dsDNA conjugate, will lead to pattern eradication. As for the assessment of the DNA duplex binding affinity, we also confirmed the visual observation of pattern alteration until its extinction by image autocorrelation (Figure 3d). Intriguingly, one can clearly recognize the receding pattern density due to increasing inhibitor addition, thus facilitating the evaluation of inhibitor strength. IC_{50} values of 551 nM (95% CI of 393.6 to 772.0 nM) for the 10-mer and 2062.0 nM (95% CI: 1557.0 to 2730.0 nM) for the 7-mer were determined from MinD ATPase activity (Figure 3b). In summary, these results indicate that it is possible to screen for inhibitory modulators with diverse affinities with our assay. Advantageously, screening for modulators can be performed immediately after the evaluation of the targeted interaction partners, reducing operational time and reagent consumption compared to other assays.[23]

Adaptability of Assay for Screening Other Biomolecules. So far, we have used DNA handles as tractable model interaction pairs to characterize our assay. To test the applicability of our assay to other molecules, such as peptides and proteins, we also investigated other model interaction partners. First, we focused on the ubiquitous family of basic Leucine Zipper Domain (bZIP) transcription factors (TFs), which confer function (DNA binding) through dimerization of the bZIP domains. A particular feature of this TF class is the conformability as a result of bZIP interaction partner selection, leading to various event cascades that are, e.g., crucial for cell differentiation of proliferation.[24] In particular, we made use of several recently published bZIP domains that were based on a

https://dx.doi.org/10.1021/acs.bioconjchem.0c00596
Bioconjugate Chem. 2021, 32, 172−181

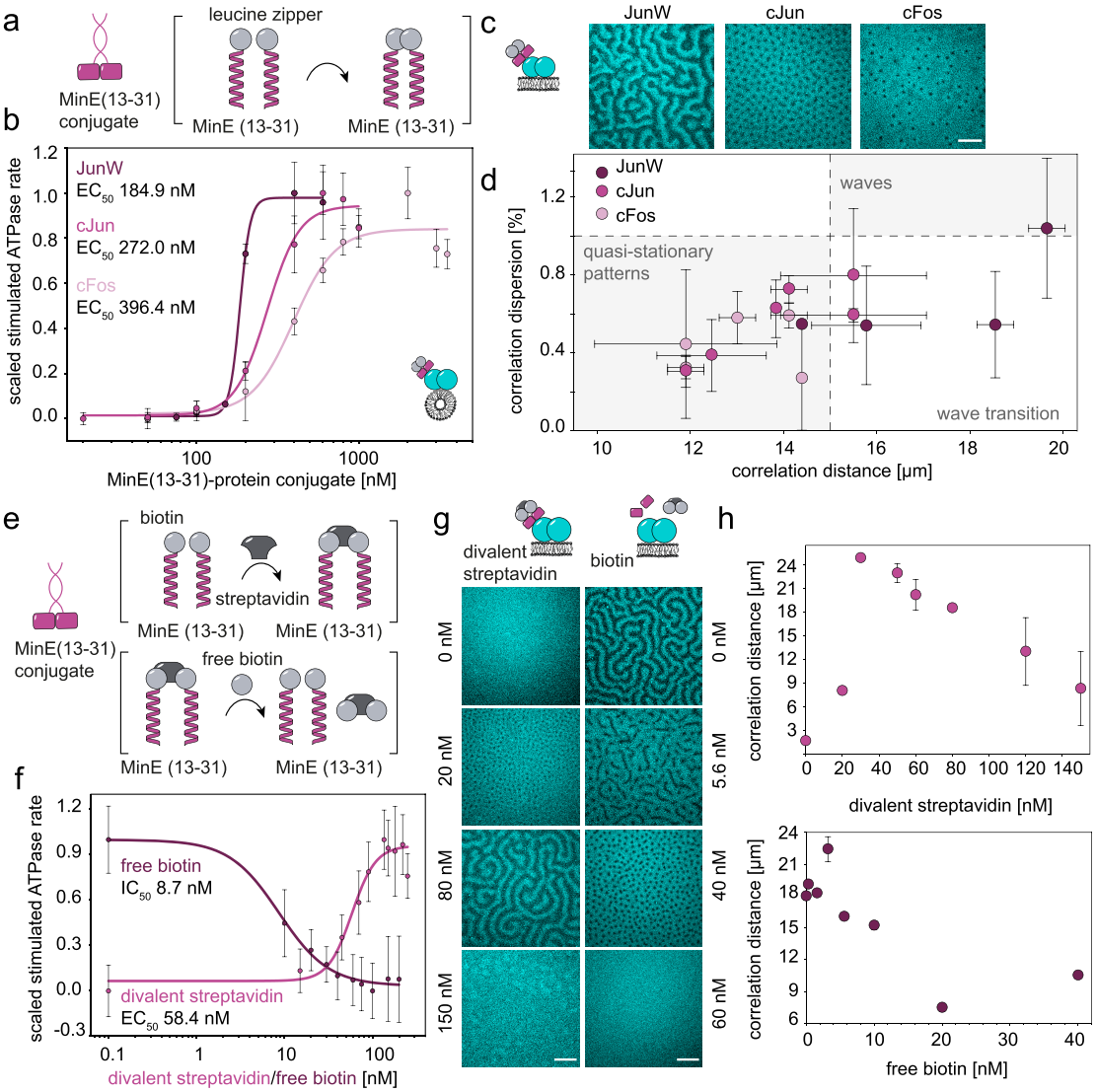

Figure 4. MinE(13−31) peptide can act as a versatile sensor to assess biomolecular dimerization, chemically induced interactions or even the inhibitory effect of agents on preformed complexes. (a) Graphic model of a minimal MinE-conjugate comprising the MinE(13−31) peptide fused to leucine zipper sequences that enable homo- or heterodimerization. (b) Enzymatic activity of MinD ATPase ratein response to the addition of the three examined leucine zipper-peptide conjugates. Plotted values (JunW − dark purple, cJun − purple, cFos − mauve) represent the mean ± SD of two independent assays, each comprising three technical replicates. JunW − EC_{50} 184.9 nM with a 95% CI of 177.3 to 192.9 nM; cJun − EC_{50} 272.0 nM with a 95% CI of 244.0 to 303.3 nM and cFos − EC_{50} 396.4 nM with a 95% CI of 349.5 to 449.7 nM. (c) Fluorescent images illustrating the self-organization of MinD with 200 nM of the leucine zipper-peptide conjugates JunW, cJun, or cFos. (d) Classification of the obtained leucine-zipper-peptide conjugate induced MinD-patterns according to the correlation distance and the determined correlation dispersion. Each two replicates per MinE(13−31)-leucine zipper conjugate and concentration were analyzed (data representation: mean ± SD). A visual overview of the obtained patterns is shown in Figure S9 and images displaying no patterns were excluded for every conjugate pair (correlation distance <4 μm). (e) Schematic illustration of a MinE(13−31)-peptide fusion construct with an attached biotin moiety on the N-terminus of the peptide (upper panel). This modification enables the dimerization of the MinE peptide in response to the addition of divalent streptavidin. Lower panel: illustration of the outcompetition of MinE(13−31)−biotin/divalent streptavidin complexes with free biotin in solution. (f) Stimulation and inhibition of MinD enzymatic activity in response to either the addition of divalent streptavidin (500 nM MinE(13−31)−biotin; pink; EC50−58.4 nM with a 95% CI of 47.8 to 71.5 nM) or free biotin (500 nM MinE(13−31)−biotin, 90 nM divalent streptavidin; dark purple; IC_{50} − 8.7 nM with a 95% CI of 5.3 to 14.1 nM), respectively. Plotted values represent the mean ± SD of two independent assays, each comprising three technical replicates. (g) Representative fluorescent images depicting MinD pattern formation, stimulated through 500 nM MinE(13−31)−biotin and varying concentrations of divalent streptavidin (left panel). Right panel: Receding MinD self-organization (MinD, 500 nM MinE(13−31)−biotin and 90 nM divalent streptavidin) due to the addition of free biotin that competes for streptavidin binding with the biotin−peptide conjugate. All *in vitro* reconstitution experiments depicted were performed with 1 μM MinD doped with 30% ATTO655-KCK-MinD, were at least carried out in duplicate, and scale bars represent 40 μm. (h) Image analysis of divalent streptavidin stimulated MinD self-organization (upper panel) or receding pattern formation due to increasing concentrations of free biotin (lower panel). For each stimulant (streptavidin) or inhibitor (free biotin), the respective concentration was plotted against the correlation distance. A visual overview of the obtained patterns is shown in Figure S10. Data represents the mean ± SD value of two independent replicates.

semirational imitation of the coiled coil (CC) regions of the activator protein-1 (AP-1).[25]

We selected three candidate CC designs (cFos, cJun, and JunW) with differing intrinsic homodimer affinities and fused

https://dx.doi.org/10.1021/acs.bioconjchem.0c00596
Bioconjugate Chem. 2021, 32, 172−181

each of them to the minimal MinE peptide (aa 13−31) before testing the resulting fusions in our assay system (Figure 4a). All three fusion constructs induced protein self-organization (Figure 4c). However, pattern onset and pattern phenotypes were found to differ, with planar surface waves induced by the JunW hybrid, and periodically distributed spots for both the cFos and cJun fusions (Figure 4d, Figure S9). Notably, the same phenotype dependence was seen for the strong (waves) or weak (hexagonal lattice) DNA-handle constructs described above. Thus, one can conclude that pattern types in fact represent a distinctive parameter for the assessment of interaction strength, regardless of the utilized moiety system. We further determined the EC_{50} values for MinD ATPase activity with respect to increasing concentrations of the CC fusion constructs. As expected, JunW was found to possess the lowest EC_{50} value (184.9 nM, 95% CI: 177.3 to 192.9 nM), while cJun (272 nM, 95% CI: 244.0 to 303.3 nM) and cFos (396 nM, 95% CI: 349.5 to 449.7 nM) had progressively higher values (Figure 4b). These values also correlate well with determined stability values that indicate the same ranking of the evaluated zipper moieties, with JunW the most stable, followed by cJun and with cFos the weakest of the three.[25]

One further class of biomolecular interaction of particular importance for basic research and drug development is that of protein−small molecule interactions (PSMIs).[26] We thus used our assay to characterize one of the predominant model systems of modern nanoscale drug delivery approaches,[27] the avidin−biotin interaction pair. Known as one of the strongest naturally occurring noncovalent interactions, this molecular pair relies on the strong cooperation of the tetrameric avidin's individual binding pockets with the small molecule biotin. We have imposed on this synergy to mimic one of the potential applications of our *in vitro* setup, the assessment of chemically induced interactions.[28] To this end, we fused a biotin moiety to the minimal MinE peptide and used a divalent streptavidin[29] to simplify reaction stoichiometry (Figure 4e). As seen with the other high-affinity interaction pairs tested above, propagating surface waves emerged at low streptavidin conditions (Figure 4g, left panel). Intriguingly, pattern development is represented nicely by the correlation distance, which initially rises due to wave evolution and subsequently decreases over the course of self-organization extinction (Figure 4h, upper panel). The thus-indicated strong affinity between the streptavidin "linker" and the two minimal MinE-biotin modules was similarly reflected in the low EC_{50} value (58.4 nM; 95% CI: 47.8 to 71.5 nM) obtained by titrating the respective components to MinD (Figure 4f).

Finally, we used this interaction system as a model to demonstrate the ability to measure the inhibitory effect of agents on preformed complexes. Namely, we used free biotin to compete with the peptide-fused biotin for binding of the divalent streptavidin (Figure 4e). Altered pattern phenotypes occurred in the presence of extremely low biotin concentrations (<10 nM), and complete abolition of patterns was observed at approximately 50 nM of biotin (Figure 4g, right panel; Figure 4h, lower panel). These observations are again supported by the low IC_{50} value (8.7 nM) obtained from the measurement of MinD ATPase activity (Figure 4f). With regard to the difference between the obtained EC_{50} and the IC_{50} value, the peptide may impose some degree of steric hindrance that could influence the affinity of the conjugated biotin vs free biotin.

CONCLUSION

We describe here an *in vitro* interaction assay harnessing protein self-organization and pattern formation as a visual readout. As the essential component, we utilized a small MinE-derived peptide, which can be simply modified, for example, by click chemistry, with any (bio)chemical moiety of interest. We found that the affinity between the examined peptide-fused moieties directly correlates with the emerging pattern type and the half-maximal enzyme-dependent ATP consumption (EC_{50}). Together with minimal reaction components, a time-stable reaction mechanism and the potential to scale up reaction throughput by automatization, our assay has the potential to be applied to high-throughput primary screening of interaction partners or compounds that might act as an inhibitor of dimerization. It would also be interesting to explore the potential application of our assay to folding state and distance dependent domain interactions. Finally, optimization of the minimal-MinE peptide in terms of helix stability, MinD binding strength, and peptide sequence length might provide improved variants that allow even further reduced concentration ranges of the biochemical moieties under investigation to be used.

EXPERIMENTAL SECTION

Plasmid Design and Molecular Cloning. To generate MinE(13−31)-leucine zipper fusion constructs, seamless assembly was performed with pET28a_MinE 13−31-Fos[6] as backbone template and the gene fragments for cJun, JunW, and cFos (Eurofins Scientific, Ebersberg, Germany) as inserts. Please refer to the Supporting Information for a detailed description of all cloning steps and a table indicating the peptide sequences (Table S1). All generated plasmids were sequenced to ensure their integrity, and a list of all generated plasmids with their respective primers can be found in Tables S4 and S5. Both pET21a-Streptavidin-Alive and pET21a-Streptavidin-Dead were a gift from Alice Ting (Addgene plasmid # 20860).[29]

Protein Purification. MinD was expressed and purified as previously described in Ramm et al.,[12] MinE(13−31)-leucine zipper fusion constructs were purified according to Glock et al.,[6] and divalent streptavidin was prepared according to Howarth et al.[29] For more detailed protocols regarding the expression and purification of all proteins mentioned above, please refer to the Supplementary Methods.

The purity and integrity of all proteins were assessed by SDS-PAGE and LC-MS. Protein concentrations were determined using a customized Bradford assay (Bio-Rad Protein Assay; Bio-Rad Laboratories Inc., Hercules, CA, USA), and the degree of labeling was estimated by UV−vis spectroscopy (V-650 spectrophotometer, Jasco, Pfungstadt, Germany). All proteins were flash-frozen in liquid nitrogen and stored as single-use aliquots at −80 °C.

Protein Labeling. Labeling of KCK-MinD with ATTO 655-maleimide (ATTO-TEC GmbH, Siegen, Germany) was performed according to the manufacturer's instruction and with a ratio of three molecules of dye per protein. Excess dye was removed by gel-filtration chromatography on a 16/600 Superdex 200 pg column (GE Healthcare, Pittsburgh, 492 USA), using an Äkta Pure chromatography system (GE Healthcare, Pittsburgh, USA) and storage buffer (50 mM HEPES pH 7.25, 150 mM KCl, 0.1 mM EDTA, 10% glycerol, 0.4 mM TCEP, 0.2 mM ADP) as mobile phase.

https://dx.doi.org/10.1021/acs.bioconjchem.0c00596
Bioconjugate Chem. 2021, 32, 172−181

Peptides. The common peptide MinE(13−31), N-term-NTANIAKERLQIIVAERRRGSGK(N3)-C-term, was synthesized by our in-house Biochemistry Core Facility or biomers.net GmbH (Ulm, Germany) using standard Fmoc chemistry. Peptide−ssDNA conjugates were assembled via copper-free click chemistry between the azidolysine and the 5′-dibenzocyclooctyne (DBCO) of the ssDNA (performed by biomers.net GmbH). D(+)-Biotin (Merck KGaA, Darmstadt, Germany) was used to biotinylate the azidolysine (in-house Biochemistry Core Facility). Detailed information regarding syntheses performed in-house is provided in the Supporting Information. All peptide conjugates (Table S2) were resuspended in ultrapure (Milli-Q) water and stored as 10 μL aliquots at −20 °C.

ssDNA. ssDNAs for competition assays were purchased from Eurofins Scientific (Ebersberg, Germany) and purified by HPLC.

ADP/ATP Stock Solution. ADP/ATP stocks were prepared from their respective disodium salt hydrates (Sigma-Aldrich, St. Louis, USA), supplemented with an equal amount of $MgCl_2$ and adjusted to pH 7.5. Nucleotide concentration was spectroscopically determined from the absorbance at 259 nm (V-650; Jasco, Pfungstadt, Germany) using an extinction coefficient of 15,400 M^{-1} cm^{-1}.

Preparation of Small Unilamellar Vesicles (SUVs). The lipids dioleoyl-*sn*-glycero-3-phosphocholine (DOPC) and dioleoyl-*sn*-glycero-3-phosphoglycerol (DOPG) (Avanti Polar Lipids, Alabaster, USA) were dissolved in chloroform (Sigma-Aldrich, St. Louis, USA) and mixed in a ratio of 70 mol % DOPC to 30 mol % DOPG. Solvent was evaporated under a nitrogen stream followed by removal of residual chloroform for 1 h in a vacuum desiccator. The dried lipid film was then hydrated with Min buffer (25 mM Tris HCl, pH 7.5, 150 mM KCl, 5 mM $MgCl_2$). SUVs were formed by performing consecutive freeze−thawing cycles (8−10) using liquid nitrogen and a 90 °C water bath. To obtain monodisperse vesicles, the vesicle mixture was then extruded through a Whatman nucleopore membrane (GE Healthcare, Chicago, USA) with a pore size of 50 nm, for 37 passes. After preparation, vesicles for NADH-coupled ATPase assays were used immediately.

NADH Coupled ATPase Assay. To determine the ability of the generated peptide-ssDNA and peptide−leucine zipper conjugates to stimulate MinD ATPase activity, we performed an NADH-coupled ATPase assay which connects the reaction of ADP with PEP to pyruvate and ATP, followed by the reduction of pyruvate using NADH to L-lactate and NAD^+. This assay was also used to assess the ability of competitor ssDNA to inhibit the stimulation of MinD ATPase activity through peptide−ssDNA conjugates. All assays were performed in Min buffer (25 mM Tris HCl, pH 7.5, 150 mM KCl, 5 mM $MgCl_2$) and all reagents were purchased from Sigma-Aldrich (St. Louis, USA). To monitor the decrease in NADH concentration over time, 2 mM phosphoenolpyruvate (PEP), 0.5 mM reduced nicotinamide adenine dinucleotide (NADH), 0.2 mg/mL extruded SUVs (ø 50 nm), 4.5 μL of a commercial enzyme mix containing pyruvate kinase (600−1000 U/mL) and lactate dehydrogenase (1000−1400 U/mL) and 1 μM MinD where put together with the peptide-fusion constructs of interest. All reagents were carefully mixed and adjusted to a final reaction volume of 150 μL in a 96-well plate. NADH absorption was followed at 340 nm in a Spark multimode microplate reader (Tecan Group Ltd., Männedorf, Switzerland) and wells devoid of proteins were used to compensate for NADH decomposition due to reasons other than MinD ATPase activity. If not indicated otherwise, assays were performed in duplicate with each comprising three technical replicates (n = 6).

Supported Lipid Bilayer (SLB) Formation. Supported lipid bilayers (SLBs) were formed by fusion of SUVs in a 96-well plate with a glass bottom (Greiner Bio-One, Kremsmünster, Austria). Plates were cleaned for 30 s (30% power, 0.3 mbar) in a Zepto plasma cleaner (Diener electronic GmbH, Ebhausen, Germany) using oxygen as the process gas. Lipids were prepared as described above, except that sonication was used instead of freeze−thaw cycles to form SUVs. SUVs were added to each reaction chamber at a final concentration of 0.6 mg/mL and incubated for 2 min on a 37 °C warm heating block. Unfused SUVs were then removed through subsequent washing with SLB buffer (25 mM Tris-HCl pH 7.5, 150 mM KCl), and after cooling to room temperature, SLB buffer was exchanged to Min buffer (25 mM Tris-HCl pH 7.5, 150 mM KCl, 5 mM $MgCl_2$).

Self-Organization Assay. All self-organization assays were performed as previously described.[12,30] Briefly, MinD and MinE(13−31)ssDNA or leucine zipper conjugates were added together with 2.5 mM ATP (final concentration) to an SLB reaction chamber containing a reaction volume (Min buffer; 25 mM Tris HCl, pH 7.5, 150 mM KCl, 5 mM $MgCl_2$) of 200 μL. For fluorescence imaging, MinD was doped with 30% ATTO655-KCK-MinD. For ssDNA-competition assays, 160 nM of the common 10 nt peptide and the 10 nt peptide conjugate were preincubated with 1 μM MinD to induce self-organization prior to the addition of the 12-mer, the 10-mer, or the 7-mer ssDNA.

Microscopy. Imaging was performed on either a commercial Zeiss LSM800 or LSM780 confocal microscope each equipped with a Zeiss C-Apochromat 40X/1.20 water-immersion objective (Carl Zeiss AG, Oberkochen, Germany). ATTO655-KCK-MinD was excited at 640 nm and imaging was performed with a pinhole diameter of 1 Airy unit. Image recording was performed with a scan rate of 2.06 μs per pixel.

Image Analysis. Image analysis was performed in Fiji with the Radial Profile plugin (https://imagej.nih.gov/ij/plugins/radial-profile.html) using custom macro scripts.[31,32] To discriminate among different patterns and to further characterize them, two approaches were applied. In the first, autocorrelation analysis was performed for each image. A soft windowing function (raised-cosine window, 1 at the center and 0.75 at the edges) was applied to reduce edge effects. Then the autocorrelation image was computed, from which a radial amplitude profile was generated. The position of the first peak in the profile was identified as the correlation distance. Patterns were further analyzed by computing the percentage variation of the correlation intensity along the ring in the autocorrelation image, here defined as correlation dispersion. For pattern classification, a scatter plot of the correlation distance against the dispersion was used to assign the images into three categories: quasi-stationary, wave transition, and traveling surface waves. Once separated, the pattern types were further characterized on the basis of additional parameters. Specifically, for the quasi-stationary patterns we used the spot density, derived from the reciprocal of the squared correlation distance, or the correlation distance itself. The antagonist strength of the wave images was characterized by the coefficient of variation, i.e., the normalized variance computed over the image, which is

https://dx.doi.org/10.1021/acs.bioconjchem.0c00596
Bioconjugate Chem. 2021, 32, 172−181

a measure of the relative contrast. Small protein aggregates, when present in the field of view, were computationally removed (remove outliers function in Fiji) before determining the coefficient of variation, to avoid bias in the statistics. All microscope images presented in both the main text and the Supporting Information have been uniformly adjusted for brightness and contrast using Fiji.

Data Analysis. Data processing, analysis, and graph plotting was performed with GraphPad Prism (GraphPad Software, ver. 8.0). To determine the halfway response (EC_{50}) to the stimulation with the MinE peptide versions a log(agonist) vs response fit (variable slope with four parameters) was used to analyze the generated ATPase rate curves. For competitor assays, the IC_{50} was determined using a log(inhibitor) vs response fit (variable slope with four parameters).

■ ASSOCIATED CONTENT

Supporting Information

The Supporting Information is available free of charge at https://pubs.acs.org/doi/10.1021/acs.bioconjchem.0c00596.

Supporting methods with associated figures and tables (PDF)

■ AUTHOR INFORMATION

Corresponding Author

Petra Schwille − *Department of Cellular and Molecular Biophysics, Max Planck Institute of Biochemistry, 82152 Planegg, Germany;* orcid.org/0000-0002-6106-4847; Phone: +49 89 8578-2900; Email: schwille@biochem.mpg.de; Fax: +49 89 8578-2903

Authors

Tamara Heermann − *Department of Cellular and Molecular Biophysics, Max Planck Institute of Biochemistry, 82152 Planegg, Germany;* orcid.org/0000-0003-1607-0727

Henri G. Franquelim − *Department of Cellular and Molecular Biophysics, Max Planck Institute of Biochemistry, 82152 Planegg, Germany;* orcid.org/0000-0001-6229-4276

Philipp Glock − *Department of Cellular and Molecular Biophysics, Max Planck Institute of Biochemistry, 82152 Planegg, Germany*

Leon Harrington − *Department of Cellular and Molecular Biophysics, Max Planck Institute of Biochemistry, 82152 Planegg, Germany;* orcid.org/0000-0002-6781-2367

Complete contact information is available at: https://pubs.acs.org/10.1021/acs.bioconjchem.0c00596

Author Contributions

T.H., H.G.F., and P.S. conceived the study. T.H. designed, performed and analyzed all experiments. P.G. and L.H. assisted with initial experiments. T.H. wrote the manuscript draft and all authors revised, reviewed and approved the manuscript.

Notes

The authors declare no competing financial interest.

■ ACKNOWLEDGMENTS

We thank G. Cardone (MPIB Imaging Facility) for assistance with image analysis, K. Andersson and the MPIB Core Facility for assistance with protein purification, and K. Nakel for assistance with ATPase assays. We also thank S. Pettera (MPIB Core Facility) for peptide synthesis, M. Schaper for assistance with cloning, B. Ramm for providing divalent streptavidin and helpful discussions, and S. Bauer for vesicle preparation. T.H. and P.S. acknowledge funding by the Deutsche Forschungsgemeinschaft (DFG, German Research Foundation) − Project-ID 201269156 − SFB 1032 (A09) and H.G.F. and P.S. through Project-ID 111166240 − SFB 863. Additional support was provided by the Center for NanoScience (CeNS), Center for Integrated Protein Science Munich (CIPSM), and Nanosystems Initiative Munich (NIM) and H.G.F. was awarded a Humboldt Research Fellowship (PTG/1152511/STP) from the Alexander von Humboldt Foundation. P.G. acknowledges support by the International Max-Planck Research School for Molecular Life Sciences (IMPRS-LS) as well as financial support by the DFG Research Training Group GRK2062 ("Molecular Principles of Synthetic Biology"). L.H. thanks the European Union's Horizon 2020 research and innovation program for a Marie Skłodowska-Curie grant (705587), and the Humboldt Foundation for a fellowship. P.S. further acknowledges support through the research network MaxSynBio via the joint funding initiative of the German Federal Ministry of Education and Research (BMBF) as well as the Max Planck Society.

■ ABBREVIATIONS

bZIP, Basic Leucine Zipper Domain; CoV, coefficient of variation; CC, coiled coil; CI, confidence interval; DBCO, dibenzocyclooctyne; DOPC, dioleoyl-*sn*-glycero-3-phosphocholine; DOPG, dioleoyl-*sn*-glycero-3-phosphoglycerol; FCS, fluorescence correlation spectroscopy; FRET, Förster resonance energy transfer; ITC, isothermal titration calorimetry; MTS, membrane targeting sequence; NADH, nicotinamide adenine dinucleotide; PEP, phosphoenolpyruvate; PSMI, protein small molecule interactions; RD, reaction-diffusion; SLB, supported lipid bilayer; SUVs, small unilamellar vesicles; ssDNA, single-stranded DNA; TF, transcription factor.

■ REFERENCES

(1) Dixon, A. S., Schwinn, M. K., Hall, M. P., Zimmerman, K., Otto, P., Lubben, T. H., Butler, B. L., Binkowski, B. F., MacHleidt, T., Kirkland, T. A., et al. (2016)et al NanoLuc Complementation Reporter Optimized for Accurate Measurement of Protein Interactions in Cells. *ACS Chem. Biol. 11* (2), 400−408.

(2) Younger, D., Berger, S., Baker, D., and Klavins, E. (2017) High-Throughput Characterization of Protein−Protein Interactions by Reprogramming Yeast Mating. *Proc. Natl. Acad. Sci. U. S. A. 114* (46), 12166−12171.

(3) Fields, S., and Song, O. K. (1989) A Novel Genetic System to Detect Protein-Protein Interactions. *Nature 340* (6230), 245−246.

(4) Ullman, E. F., Kirakossian, H., Singh, S., Wu, Z. P., Irvin, B. R., Pease, J. S., Switchenko, A. C., Irvine, J. D., Dafforn, A., Skold, C. N., et al. (1994)et al Luminescent Oxygen Channeling Immunoassay: Measurement of Particle Binding Kinetics by Chemiluminescence. *Proc. Natl. Acad. Sci. U. S. A. 91* (12), 5426−5430.

(5) Gell, D. A., Grant, R. P., and MacKay, J. P. (2012) The Detection and Quantitation of Protein Oligomerization. *Adv. Exp. Med. Biol. 747*, 19−41.

(6) Glock, P., Brauns, F., Halatek, J., Frey, E., and Schwille, P. (2019) Design of Biochemical Pattern Forming Systems from Minimal Motifs. *eLife 8*, 1.

(7) Camazine, S., Franks, N., and Sneyd, J. (2001) *Self-Organization in Biological Systems*, Princeton University Press, Princeton.

(8) de Boer, P. A. J., Crossley, R. E., and Rothfield, L. I. (1989) A Division Inhibitor and a Topological Specificity Factor Coded for by

the Minicell Locus Determine Proper Placement of the Division Septum in E. Coli. *Cell 56* (4), 641−649.
(9) Kretschmer, S., Zieske, K., and Schwille, P. (2017) Large-Scale Modulation of Reconstituted Min Protein Patterns and Gradients by Defined Mutations in MinE's Membrane Targeting Sequence. *PLoS One 12* (6), e0179582.
(10) Glock, P., Broichhagen, J., Kretschmer, S., Blumhardt, P., Mücksch, J., Trauner, D., and Schwille, P. (2018) Optical Control of a Biological Reaction−Diffusion System. *Angew. Chem., Int. Ed. 57* (9), 2362−2366.
(11) Vecchiarelli, A. G., Li, M., Mizuuchi, M., Hwang, L. C., Seol, Y., Neuman, K. C., and Mizuuchi, K. (2016) Membrane-Bound MinDE Complex Acts as a Toggle Switch That Drives Min Oscillation Coupled to Cytoplasmic Depletion of MinD. *Proc. Natl. Acad. Sci. U. S. A. 113* (11), E1479−E1488.
(12) Ramm, B., Glock, P., and Schwille, P. (2018) In Vitro Reconstitution of Self-Organizing Protein Patterns on Supported Lipid Bilayers. *J. Visualized Exp.* No. 137, 1−13.
(13) Ramm, B., Heermann, T., and Schwille, P. (2019) The E. Coli MinCDE System in the Regulation of Protein Patterns and Gradients. *Cell. Mol. Life Sci. 76* (21), 4245−4273.
(14) Park, K.-T., Wu, W., Battaile, K. P., Lovell, S., Holyoak, T., and Lutkenhaus, J. (2011) The Min oscillator uses MinD-dependent conformational changes in MinE to spatially regulate cytokinesis. *Cell 146*, 396−407.
(15) Ghasriani, H., and Goto, N. K. (2011) Regulation of Symmetric Bacterial Cell Division by MinE What Is the Role of Conformational Dynamics? *Commun. Integr. Biol. 4* (1), 101−103.
(16) Duff, M. R., Grubbs, J., and Howell, E. E. (2011) Isothermal Titration Calorimetry for Measuring Macromolecule-Ligand Affinity. *J. Visualized Exp. 55* (55), 2796.
(17) Kondo, S., and Miura, T. (2010) Reaction-Diffusion Model as a Framework for Understanding Biological Pattern Formation. *Science 329* (5999), 1616−1620.
(18) Shoji, H., Iwasa, Y., and Kondo, S. (2003) Stripes, Spots, or Reversed Spots in Two-Dimensional Turing Systems. *J. Theor. Biol. 224* (3), 339−350.
(19) Halatek, J., and Frey, E. (2012) Highly Canalized MinD Transfer and MinE Sequestration Explain the Origin of Robust MinCDE-Protein Dynamics. *Cell Rep. 1* (6), 741−752.
(20) Zheng, M., Chiang, Y. L., Lee, H. L., Kong, L. R., Hsu, S. T. D., Hwang, I. S., Rothfield, L. I., and Shih, Y. L. (2014) Self-Assembly of MinE on the Membrane Underlies Formation of the MinE Ring to Sustain Function of the Escherichia Coli Min System. *J. Biol. Chem. 289* (31), 21252−21266.
(21) Hanahan, D., and Weinberg, R. A. (2011) Hallmarks of Cancer: The next Generation. *Cell 144* (5), 646−674.
(22) Arkin, M. R., Glicksman, M. A., Fu, H., Havel, J. J., and Du, Y. (2004) *Inhibition of Protein-Protein Interactions: Non-Cellular Assay Formats*, PubMed.gov.
(23) Al-Mugotir, M., Kolar, C., Vance, K., Kelly, D. L., Natarajan, A., and Borgstahl, G. E. O. (2019) A Simple Fluorescent Assay for the Discovery of Protein-Protein Interaction Inhibitors. *Anal. Biochem. 569*, 46−52.
(24) Amoutzias, G. D., Robertson, D. L., Van de Peer, Y., and Oliver, S. G. (2008) Choose Your Partners: Dimerization in Eukaryotic Transcription Factors. *Trends Biochem. Sci. 33* (5), 220−229.
(25) Mason, J. M., Schmitz, M. A., Muller, K. M., and Arndt, K. M. (2006) Semirational Design of Jun-Fos Coiled Coils with Increased Affinity: Universal Implications for Leucine Zipper Prediction and Design. *Proc. Natl. Acad. Sci. U. S. A. 103* (24), 8989−8994.
(26) Mcfedries, A., Schwaid, A., and Saghatelian, A. (2013) Chemistry & Biology Review Methods for the Elucidation of Protein-Small Molecule Interactions. *Chem. Biol. 20*, 667−673.
(27) Jain, A., and Cheng, K. (2017) The Principles and Applications of Avidin-Based Nanoparticles in Drug Delivery and Diagnosis Graphical Abstract HHS Public Access. *J. Controlled Release 245*, 27−40.
(28) Stanton, B. Z., Chory, E. J., and Crabtree, G. R. (2018) Chemically Induced Proximity in Biology and Medicine. *Science 359* (6380), eaao5902.
(29) Howarth, M., and Ting, A. (2008) Monovalent Streptavidin Expression and Purification. *Nat. Protoc. 3*, 534.
(30) Loose, M., Fischer-Friedrich, E., Ries, J., Kruse, K., and Schwille, P. (2008) Spatial Regulators for Bacterial Cell Division Self-Organize into Surface Waves in Vitro. *Science 320* (5877), 789−792.
(31) Schindelin, J., Arganda-Carreras, I., Frise, E., Kaynig, V., Longair, M., Pietzsch, T., Preibisch, S., Rueden, C., Saalfeld, S., Schmid, B., et al. (2012)etal Fiji: An Open-Source Platform for Biological-Image Analysis. *Nat. Methods 9* (7), 676−682.
(32) Schneider, C. A., Rasband, W. S., and Eliceiri, K. W. (2012) NIH Image to ImageJ: 25 Years of Image Analysis. *Nat. Methods 9* (7), 671−675.

https://dx.doi.org/10.1021/acs.bioconjchem.0c00596
Bioconjugate Chem. 2021, 32, 172−181